

# General relativity and cosmic structure formation

Julian Adamek<sup>1</sup>, David Daverio<sup>1</sup>, Ruth Durrer<sup>1</sup> & Martin Kunz<sup>1,2</sup>

<sup>1</sup> Département de Physique Théorique & Center for Astroparticle Physics, Université de Genève, 24 Quai E. Ansermet, 1211 Genève 4, Switzerland

<sup>2</sup> African Institute for Mathematical Sciences, 6 Melrose Road, Muizenberg 7945, South Africa

September 8, 2015

## Abstract

Numerical simulations are a versatile tool providing insight into the complicated process of structure formation in cosmology [1]. This process is mainly governed by gravity, which is the dominant force on large scales. To date, a century after the formulation of general relativity [2], numerical codes for structure formation still employ Newton’s law of gravitation. This approximation relies on the two assumptions that gravitational fields are weak and that they are only sourced by non-relativistic matter. While the former appears well justified on cosmological scales, the latter imposes restrictions on the nature of the “dark” components of the Universe (dark matter and dark energy) which are, however, poorly understood. Here we present the first simulations of cosmic structure formation using equations consistently derived from general relativity. We study in detail the small relativistic effects for a standard  $\Lambda$ CDM cosmology which cannot be obtained within a purely Newtonian framework. Our particle-mesh N-body code computes all six degrees of freedom of the metric and consistently solves the geodesic equation for particles, taking into account the relativistic potentials and the frame-dragging force. This conceptually clean approach is very general and can be applied to various settings where the Newtonian approximation fails or becomes inaccurate, ranging from simulations of models with dynamical dark energy [3] or warm/hot dark matter [4] to core collapse supernova explosions [5].

The applicability of Newton’s law of gravitation in the context of cosmic structure formation has been discussed extensively in the recent literature [6, 7, 8]. In particular, it is now well understood that this simplified description is quite accurate when applied within standard  $\Lambda$ CDM cosmology where perturbations come entirely from non-relativistic matter. However, the situation is not satisfactory for two reasons. Firstly, the quality of observational data is rapidly increasing, and upcoming galaxy surveys will eventually reach a precision where a naive treatment of the effects of spacetime geometry becomes insufficient [9, 10]. Secondly, the true nature of dark matter and dark energy is not yet established. In order to study models beyond  $\Lambda$ CDM, some of which may feature relativistic sources of stress-energy (e.g. warm dark matter or dynamical dark energy), employing the Newtonian approximation is not always justified. A number of numerical codes has been developed for particular models [11, 12, 13, 14], yet a general framework would be desirable. Furthermore, Newtonian gravity is acausal and not sensitive to the presence of a cosmological horizon. Even if a judicious interpretation of the output of Newtonian simulations can cure this problem at the linear level, it comes back when one goes beyond linear perturbation theory and it would be preferable to use the correct physics from the outset.

Moving from the absolute space and time of the Newtonian picture towards a general relativistic view where geometry is dynamical poses a significant conceptual challenge. Recent progress is owed to a suitable formulation of the relativistic setting in terms of a weak-field expansion which is well adapted for (but not restricted to) cosmological applications [7, 15, 16]. Based on these ideas we have developed a numerical code, `gevolution`, which is designed to perform cosmological N-body simulations fully in the context of general relativity, evolving all six metric degrees of freedom. In brief, our approach can be summarized as follows.

1. We choose a suitable ansatz for the metric which is split into background and perturbations. We work in Poisson gauge where the perturbed Friedmann-Lemaître-Robertson-Walker metric is

$$ds^2 = a^2(\tau) \left[ - (1 + 2\Psi) d\tau^2 - 2B_i dx^i d\tau + (1 - 2\Phi) \delta_{ij} dx^i dx^j + h_{ij} dx^i dx^j \right], \quad (1)$$

where  $a$  denotes the scale factor of the background,  $x^i$  are comoving coordinates on the spacelike hypersurfaces, and  $\tau$  is conformal time.  $B_i$  (also denoted as  $\mathbf{B}$ ) is transverse and is responsible for frame dragging;  $h_{ij}$  is transverse and traceless, it contains the two spin-2 degrees of freedom of gravitational waves.

2. We assume that the perturbations of the metric, but not necessarily their derivatives, remain small on the scales of interest. This is a valid approximation for cosmological scales even when perturbations in the stress-energy tensor are large.
3. Einstein’s equations are then expanded in terms of the metric perturbations but without a perturbative treatment of the stress-energy tensor. We include all terms linear in metric perturbations and go to quadratic order in terms which have two spatial derivatives acting on the scalar metric perturbations  $\Phi$ ,  $\Psi$ . This weak-field expansion contains all six components of the metric correctly at leading order. To determine the evolution of the metric, we numerically solve the “00” and the traceless part of the “ $ij$ ” Einstein equations:

$$(1 + 4\Phi) \Delta\Phi - 3\mathcal{H}\Phi' - 3\mathcal{H}^2\Psi + \frac{3}{2}(\nabla\Phi)^2 = -4\pi G a^2 \delta T_0^0, \quad (2a)$$

$$\begin{aligned} & \left( \delta_k^i \delta_l^j - \frac{1}{3} \delta_{kl} \delta^{ij} \right) \left[ \frac{1}{2} h''_{ij} + \mathcal{H} h'_{ij} - \frac{1}{2} \Delta h_{ij} + B'_{(i,j)} + 2\mathcal{H} B_{(i,j)} + (\Phi - \Psi)_{,ij} \right. \\ & \left. + (\Phi - \Psi)_{,i} (\Phi - \Psi)_{,j} + 2(\Phi - \Psi) (\Phi - \Psi)_{,ij} - 2(\Phi - \Psi) \Phi_{,ij} + 2\Phi_{,i} \Phi_{,j} + 4\Phi \Phi_{,ij} \right] \\ & = 8\pi G a^2 \left( \delta_{ik} T_l^i - \frac{1}{3} \delta_{kl} T_i^i \right). \quad (2b) \end{aligned}$$

Eq. (2a) is the generalisation of the Newtonian Poisson equation ( $\Delta\Phi = 4\pi G a^2 \delta\rho$ ) and contains additional relativistic terms. Here  $\Delta\Phi$  and  $\delta T_0^0 = -\delta\rho = T_0^0 - \bar{T}_0^0$  are not required to be small – in fact, they become much larger than the background value  $\bar{T}_0^0$  inside dense regions. Eq. (2b) can be used to evolve all the non-Newtonian degrees of freedom of the metric:  $\Phi - \Psi$ , the two spin-1 degrees of freedom,  $\mathbf{B}$ , and the two spin-2 helicities,  $h_{ij}$ . To do this, we decompose the equation into scalar, vector and tensor parts in Fourier space.

4. The metric is then used to solve the equations of motion for matter (and possibly other degrees of freedom); collisionless particles propagate along geodesics in the perturbed geometry. This determines the evolution of the stress-energy tensor.

The implementation in `gevolution` adopts a particle-mesh scheme where the metric field is represented on a regular cubic lattice while matter takes the form of an N-body ensemble of particles that samples the six-dimensional phase space. The stress-energy tensor on the lattice is obtained by a particle-to-mesh projection and is used in Einstein’s equations to solve for the metric perturbations. Finally, the particles are evolved by interpolating the metric to the particle positions and integrating the geodesic equation. `gevolution` is built on top of the `LATfield2` c++ framework [17]. `LATfield2` handles the lattice, the fields, the parallelization (using MPI) and the Fast Fourier Transforms which `gevolution` needs for solving Eqs. (2a) and (2b). We have extended the public version of `LATfield2` to also handle the N-body particles, including projection and interpolation methods. We plan to make these features publicly available in the near future, together with a release of the `gevolution` code.

As a first application we choose standard  $\Lambda$ CDM cosmology. We expect only small effects in this case, but we can use these simulations to gain confidence in our new approach. We generate [18] two halo catalogs containing  $\sim 500,000$  halos each, one using our relativistic approach and one with the traditional Newtonian approach as reference, starting from identical linear initial conditions. A Kolmogorov-Smirnov test shows no significant disagreement in the distributions of some 25 different halo properties such as mass, spin or shape parameters.

The largest non-Newtonian effect is frame dragging, which is associated with the spin-1 perturbation  $\mathbf{B}$ . This perturbation is sourced by the curl part of the momentum density found, e.g., in rotating massive objects. As long as perturbations are small this is a second-order effect which has been studied using perturbation theory [19]. The power spectrum for  $\mathbf{B}$  has also been computed in the non-perturbative regime of structure formation using a post-Newtonian framework [20] which shares some features with our approach. These results are useful benchmarks for our code, but we now go beyond: our simulations track the full three-dimensional realisation of  $\mathbf{B}$  (see Fig. 1). We can therefore measure the actual frame dragging force on individual particles.

While the typical gravitational acceleration on Mpc scales is of the order of  $10^{-9}$  cm/s<sup>2</sup>, frame dragging contributes only at the level of  $10^{-14}$  cm/s<sup>2</sup> (both numbers are mass-weighted rms values from our simulations at redshift zero), and the highest value we measure is some  $10^{-12}$  cm/s<sup>2</sup>. Thus, for objects

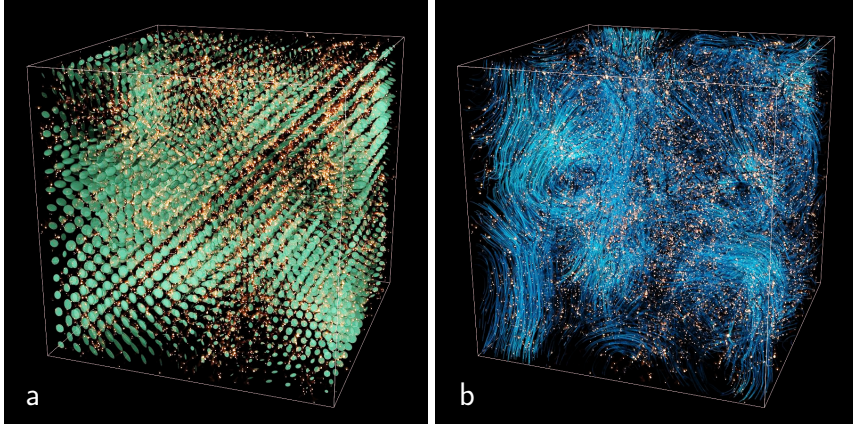


Figure 1: **Spin-1 and spin-2 metric perturbations.** Visualisation of a simulation volume of  $(512\text{Mpc}/h)^3$  at redshift  $z = 0$ . Dark matter halos are rendered as orange blobs scaled to the virial radius. Panel **a** illustrates the spin-2 perturbation  $h_{ij}$  by applying it as affine transformation on spheroids of fixed radius; the shape and size of the resulting ellipsoids therefore indicates, respectively, the polarization and amplitude of the tensor perturbation. Panel **b** shows a stream plot of the spin-1 perturbation  $\mathbf{B}$ , indicating how “spacetime is dragged around” by vortical matter flows.

moving at 1000 km/s (a typical peculiar velocity at those scales) the  $\Delta v$  due to frame dragging is no more than 1 km/s. It should be noted that these numbers are scale dependent, as the acceleration is larger on smaller scales.

We compare our simulation results also with predictions [21, 22] from second order perturbation theory for the power spectra of  $h_{ij}$ , of  $\mathbf{B}$  and of  $\Phi - \Psi$ . The latter requires regularization in the infrared, which is implemented by the finite volume of the simulation.

In order to fully capture the amplitude of the non-Newtonian terms, it is important that the scale of matter-radiation equality is represented in the simulation volume. On the other hand, these terms are generated by non-linearities and are therefore amplified at small scales. In order to obtain our results we had to cover at least three orders of magnitude in scale. Our largest simulation used a lattice with  $4096^3$  points, corresponding to  $6.7 \times 10^{10}$  particles as we always start with one particle per grid point.

Fig. 2 shows the numerical power spectra at three redshifts. For these spectra we used eight simulations with lattices of  $2048^3$  points and two different box sizes, all starting at redshift  $z = 100$ . Four simulations had a box size of  $(2048 \text{ Mpc}/h)^3$ , the other four were  $(512 \text{ Mpc}/h)^3$ . In the regime where it can be trusted we find excellent agreement with second order perturbation theory which demonstrates that our code produces valid results. At late times and on small scales, perturbation theory breaks down. Nonlinearities enhance the frame dragging by more than an order of magnitude at redshifts  $z = 1$  and  $z = 0$  and on scales  $k \gtrsim 1h/\text{Mpc}$ . The enhancement is even more dramatic for tensor perturbations.

It should finally be noted that our framework jointly solves for background and perturbations in a self-consistent way. Therefore we confirm that clustering only has a small effect on the expansion rate of the Universe. The non-Newtonian effects which we have quantified in the nonlinear regime of structure formation remain small within a  $\Lambda\text{CDM}$  Universe, but they may nevertheless be measurable in the future. For the first time, general relativity has been implemented as the theory of gravity in a cosmological N-body code, making it possible to feed these effects back into the dynamics. Our numerical framework will be particularly useful in scenarios where relativistic sources are present, like in models of dynamical dark energy, topological defects, or with relativistic particles such as neutrinos or warm dark matter. Such scenarios are expected to display larger relativistic effects. Contrary to Newtonian schemes we are also able to solve the full geodesic equation for arbitrary velocities, allowing for a realistic propagation of radiation or high-velocity particles.

## Methods

A weak-field expansion is useful in situations where the metric perturbation variables  $\Phi$ ,  $\Psi$ ,  $B_i$ ,  $h_{ij}$  defined in Eq. (1) are small, as is the case on cosmological scales. In order to get a tractable set of equations, we retain all terms which are linear in metric perturbations, but from the quadratic terms we keep only the most relevant ones. These are built from the scalar perturbations  $\Phi$ ,  $\Psi$  only, and contain the highest possible number of spatial derivatives (two in this case, since all the partial differential equations are second

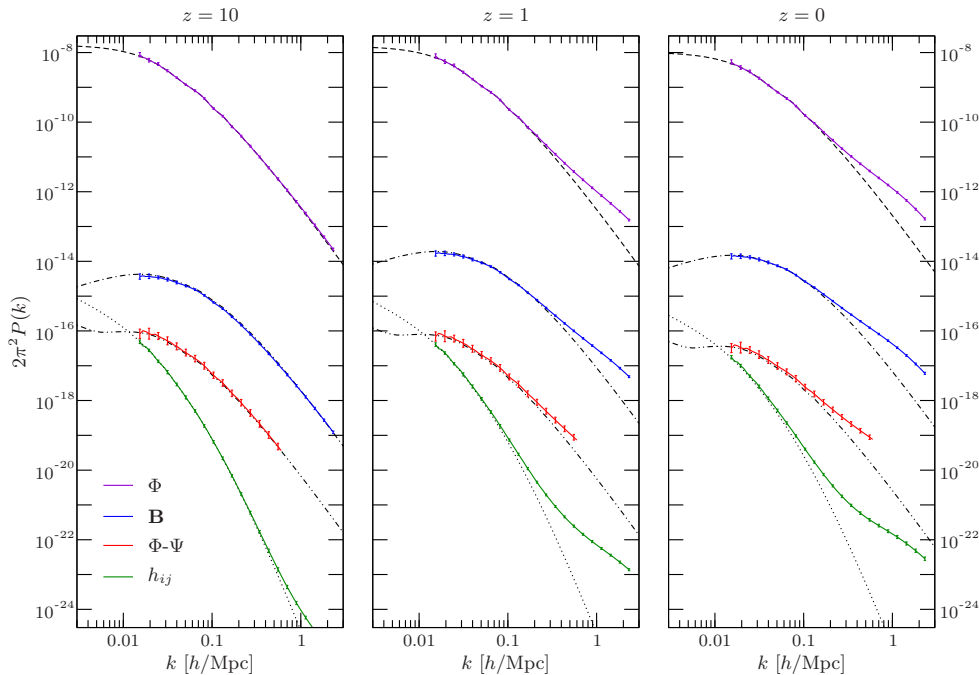


Figure 2: **Power spectra.** We show the power spectra of the gravitational potential  $\Phi$  (top, violet), the frame dragging potential  $\mathbf{B}$  (second from top, blue), the difference of the relativistic potentials  $\Phi - \Psi$  (third from top, red) and the tensor perturbation  $h_{ij}$  (bottom, green) at redshifts  $z = 10, 1, 0$ . The black lines (dashed, dot-dashed, and dotted) indicate the corresponding results from second-order perturbation theory. As expected, the numerical results deviate from these perturbative extrapolations at low redshift and small scales. All perturbation variables are significantly enhanced on scales  $k \gtrsim 1h/\text{Mpc}$  at redshift  $z = 1$  and below. Error bars indicate the random fluctuations from different realisations.

order). This is enough to ensure that all six metric degrees of freedom are treated correctly at leading order, even in cases where some of them are strongly suppressed.

**Einstein’s equations.** We determine the metric perturbations using the time-time as well as the traceless space-space part of Einstein’s equations given in Eqs. (2a) and (2b). The remaining four equations are redundant, but we can use them as consistency check. The stress-energy tensor is constructed in the perturbed geometry and may hence also contain some terms which are linear in the metric perturbations – these terms have to be taken into account in order to maintain consistency. For a  $\Lambda\text{CDM}$  cosmology as the one studied here, the stress-energy tensor is obtained numerically by appropriate particle-to-mesh projections which are “dressed” by these geometric corrections.

We then solve for the metric variables by treating the quadratic terms in Eqs. (2a) and (2b) as small perturbations. To this end, we simply estimate their value using the solutions taken from the previous time step and move them to the right-hand side. Since the equations are then approximated as linear in the metric perturbations, we can use Fourier methods to obtain the new solutions. This is convenient in particular since the gauge conditions can easily be implemented in Fourier space, where they reduce to local projection operations. One can check that the new solutions are stable by reinserting them into the quadratic terms and iterating the procedure.

**Particle trajectories.** As dark matter is assumed to be collisionless, the particles move along geodesics. For non-relativistic velocities  $\mathbf{v} = d\mathbf{x}/d\tau$  the geodesic equation reads

$$\mathbf{v}' + \mathcal{H}\mathbf{v} + \nabla\Psi - \mathcal{H}\mathbf{B} - \mathbf{B}' + \mathbf{v} \times (\nabla \times \mathbf{B}) = 0, \quad (3)$$

where the  $\mathbf{B}$ -dependent terms account for frame dragging. The integration of this equation can be simplified by writing  $\mathbf{v} = \tilde{\mathbf{v}} + \mathbf{B}$ , which transforms Eq. (3) to

$$\tilde{\mathbf{v}}' + \mathcal{H}\tilde{\mathbf{v}} + \nabla\Psi + \tilde{v}^i \nabla B_i = 0. \quad (4)$$

This new equation actually describes the acceleration as seen in a Gaussian ortho-normal coordinate frame. Frame dragging, characterized by the last term, has to compete with the “Newtonian” force  $\nabla\Psi$ . We measure both forces individually in our simulations.

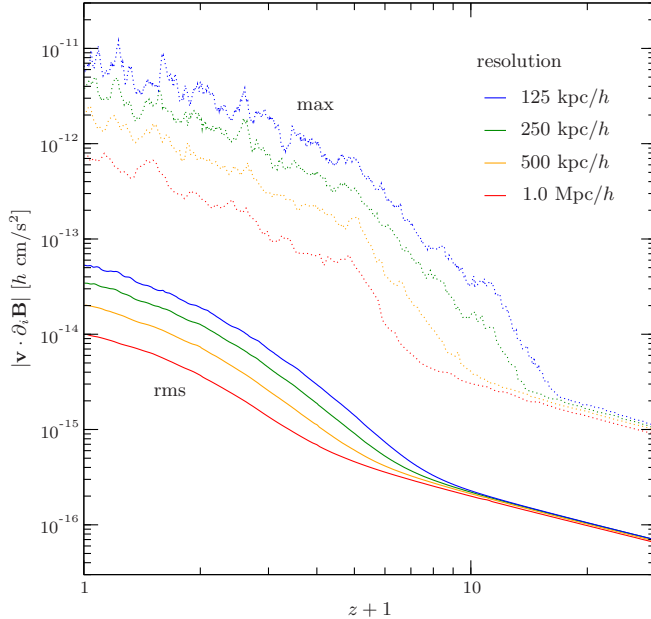


Figure 3: **Frame dragging.** We show the frame dragging acceleration as a function of redshift  $z$  as measured in simulations of different spatial resolution. The solid lines correspond to mass-weighted rms values, whereas the dotted lines indicate the maximum value measured in the simulation volume, which was fixed to  $(512 \text{ Mpc}/h)^3$ . The acceleration is scale dependent and increases with resolution. Although not shown here, we checked that the effects of finite volume and realisation scatter are less relevant.

Fig. 3 shows the mass-weighted rms value of the frame dragging acceleration ( $\tilde{\mathbf{v}} \cdot \partial_i \mathbf{B}$ ) for simulations with different spatial resolutions. The simulation volume was  $(512 \text{ Mpc}/h)^3$  in all cases, but we used lattice sizes from  $512^3$  to  $4096^3$  points, reaching a best resolution of  $125 \text{ kpc}/h$ . The rms acceleration depends on the probed scale and therefore also on resolution. At our best resolution we remain slightly above galactic scales. At smaller scales we expect baryonic effects to become important.

**Power spectra.** In Fig. 2 we show the power spectra of the metric perturbations which are defined by

$$4\pi k^3 \langle \Psi(\mathbf{k}, z) \Psi(\mathbf{k}', z) \rangle = (2\pi)^3 \delta^{(3)}(\mathbf{k} - \mathbf{k}') P_\Psi(k, z), \quad (5a)$$

$$4\pi k^3 \langle B_i(\mathbf{k}, z) B_j(\mathbf{k}', z) \rangle = (2\pi)^3 \delta^{(3)}(\mathbf{k} - \mathbf{k}') P_{ij} P_B(k, z), \quad (5b)$$

$$4\pi k^3 \langle h_{ij}(\mathbf{k}, z) h_{lm}(\mathbf{k}', z) \rangle = (2\pi)^3 \delta^{(3)}(\mathbf{k} - \mathbf{k}') M_{ijlm} P_h(k, z). \quad (5c)$$

Here  $P_{ij} = \delta_{ij} - k_i k_j / k^2$  is the transverse projector and the spin-2 projection operator is given by  $M_{ijlm} = P_{il} P_{jm} + P_{im} P_{jl} - P_{ij} P_{lm}$ . These dimensionless power spectra measure the amplitude square of the metric perturbations at scale  $k$  per  $\log k$  interval. In order to suppress finite-volume and resolution effects we only measure scales which are at least 5 times smaller than the box size and have a wave number which is at least 5 times smaller than the Nyquist frequency.

**Initial conditions.** Initial data is generated using a linear input power spectrum at initial redshift (we start at  $z = 100$ ) which can be obtained by running a Boltzmann code [23, 24] for the model. We use *CLASS* with the default cosmological parameters which describe a  $\Lambda$ CDM model ( $\Omega_b = 0.0483$ ,  $\Omega_m = \Omega_c + \Omega_b = 0.312$ , our code currently has no special treatment for baryonic matter).

**Code availability.** We will release the *gevolution* code, together with the necessary extensions of the *LATfield2* library, on a public *Git* repository (<https://github.com/gevolution-code/gevolution-1.0.git>). We strongly advise interested parties to wait for the fully documented version to become available. Prior to public release, access to the code can be given upon request, however, we do not offer extensive technical support in this case.

## Acknowledgements

We thank R. Teyssier and M. Bruni for discussions. This work was supported by the Swiss National Supercomputing Centre (CSCS) under project ID s546. The numerical simulations were carried out on

*Piz Daint* at the CSCS and on the *Baobab* cluster of the University of Geneva. Financial support was provided by the Swiss National Science Foundation.

## References

- [1] V. Springel, S. D. White, A. Jenkins, C. S. Frenk, N. Yoshida, *et al.*, “Simulating the joint evolution of quasars, galaxies and their large-scale distribution,” *Nature* **435** (2005) 629–636, [arXiv:astro-ph/0504097](#) [[astro-ph](#)].
- [2] A. Einstein, “The Field Equations of Gravitation,” *Sitzungsber.Preuss.Akad.Wiss.Berlin (Math.Phys.)* **1915** (1915) 844–847.
- [3] J. Noller, F. von Braun-Bates, and P. G. Ferreira, “Relativistic scalar fields and the quasistatic approximation in theories of modified gravity,” *Phys.Rev.* **D89** no. 2, (2014) 023521, [arXiv:1310.3266](#) [[astro-ph.CO](#)].
- [4] M. Costanzi, F. Villaescusa-Navarro, M. Viel, J.-Q. Xia, S. Borgani, E. Castorina, and E. Sefusatti, “Cosmology with massive neutrinos III: the halo mass function and an application to galaxy clusters,” *JCAP* **1312** (2013) 012, [arXiv:1311.1514](#) [[astro-ph.CO](#)].
- [5] K. Kotake, “Multiple physical elements to determine the gravitational-wave signatures of core-collapse supernovae,” *Comptes Rendus Physique* **14** (2013) 318–351, [arXiv:1110.5107](#) [[astro-ph.HE](#)].
- [6] N. E. Chisari and M. Zaldarriaga, “Connection between Newtonian simulations and general relativity,” *Phys.Rev.* **D83** (2011) 123505, [arXiv:1101.3555](#) [[astro-ph.CO](#)].
- [7] S. R. Green and R. M. Wald, “Newtonian and Relativistic Cosmologies,” *Phys.Rev.* **D85** (2012) 063512, [arXiv:1111.2997](#) [[gr-qc](#)].
- [8] G. Rigopoulos and W. Valkenburg, “On the accuracy of N-body simulations at very large scales,” *Mon.Not.Roy.Astron.Soc.* **446** (2015) 677–682, [arXiv:1308.0057](#) [[astro-ph.CO](#)].
- [9] J. Yoo and M. Zaldarriaga, “Beyond the Linear-Order Relativistic Effect in Galaxy Clustering: Second-Order Gauge-Invariant Formalism,” *Phys.Rev.* **D90** no. 2, (2014) 023513, [arXiv:1406.4140](#) [[astro-ph.CO](#)].
- [10] C. Bonvin, “Isolating relativistic effects in large-scale structure,” *Class.Quant.Grav.* **31** no. 23, (2014) 234002, [arXiv:1409.2224](#) [[astro-ph.CO](#)].
- [11] F. Schmidt, “Self-Consistent Cosmological Simulations of DGP Braneworld Gravity,” *Phys.Rev.* **D80** (2009) 043001, [arXiv:0905.0858](#) [[astro-ph.CO](#)].
- [12] B. Li, G.-B. Zhao, R. Teyssier, and K. Koyama, “ECOSMOG: An Efficient Code for Simulating Modified Gravity,” *JCAP* **1201** (2012) 051, [arXiv:1110.1379](#) [[astro-ph.CO](#)].
- [13] E. Puchwein, M. Baldi, and V. Springel, “Modified Gravity-GADGET: A new code for cosmological hydrodynamical simulations of modified gravity models,” *Mon.Not.Roy.Astron.Soc.* **436** (2013) 348, [arXiv:1305.2418](#) [[astro-ph.CO](#)].
- [14] C. Llinares, D. F. Mota, and H. A. Winther, “ISIS: a new N-body cosmological code with scalar fields based on RAMSES. Code presentation and application to the shapes of clusters,” *Astron.Astrophys.* **562** (2014) A78, [arXiv:1307.6748](#) [[astro-ph.CO](#)].
- [15] J. Adamek, D. Daverio, R. Durrer, and M. Kunz, “General Relativistic N-body simulations in the weak field limit,” *Phys.Rev.* **D88** no. 10, (2013) 103527, [arXiv:1308.6524](#) [[astro-ph.CO](#)].
- [16] J. Adamek, R. Durrer, and M. Kunz, “N-body methods for relativistic cosmology,” *Class.Quant.Grav.* **31** no. 23, (2014) 234006, [arXiv:1408.3352](#) [[astro-ph.CO](#)].
- [17] D. Daverio, M. Hindmarsh, and N. Bevis, “Latfield2: A c++ library for classical lattice field theory,” [arXiv:1508.05610](#) [[physics.comp-ph](#)].
- [18] P. S. Behroozi, R. H. Wechsler, and H.-Y. Wu, “The Rockstar Phase-Space Temporal Halo Finder and the Velocity Offsets of Cluster Cores,” *Astrophys. J.* **762** (2013) 109, [arXiv:1110.4372](#) [[astro-ph.CO](#)].
- [19] T. H.-C. Lu, K. Ananda, C. Clarkson, and R. Maartens, “The cosmological background of vector modes,” *JCAP* **0902** (2009) 023, [arXiv:0812.1349](#) [[astro-ph](#)].
- [20] M. Bruni, D. B. Thomas, and D. Wands, “Computing General Relativistic effects from Newtonian N-body simulations: Frame dragging in the post-Friedmann approach,” *Phys.Rev.* **D89** no. 4, (2014) 044010, [arXiv:1306.1562](#) [[astro-ph.CO](#)].
- [21] K. N. Ananda, C. Clarkson, and D. Wands, “The Cosmological gravitational wave background from primordial density perturbations,” *Phys. Rev.* **D75** (2007) 123518, [arXiv:gr-qc/0612013](#) [[gr-qc](#)].
- [22] D. Baumann, P. J. Steinhardt, K. Takahashi, and K. Ichiki, “Gravitational Wave Spectrum Induced by Primordial Scalar Perturbations,” *Phys.Rev.* **D76** (2007) 084019, [arXiv:hep-th/0703290](#) [[hep-th](#)].
- [23] A. Lewis, A. Challinor, and A. Lasenby, “Efficient Computation of CMB anisotropies in closed FRW models,” *Astrophys. J.* **538** (2000) 473–476, [astro-ph/9911177](#).
- [24] D. Blas, J. Lesgourgues, and T. Tram, “The Cosmic Linear Anisotropy Solving System (CLASS) II: Approximation schemes,” *JCAP* **1107** (2011) 034, [arXiv:1104.2933](#) [[astro-ph.CO](#)].